Journal of the Korean Nuclear Society
Volume 33, Number 1, pp.93 ~ 101, February, 2001

Nonlinear Dynamic Buckling Behavior of a Partial Spacer Grid Assembly

Kyung Ho Yoon, Heung Seok Kang
Hyung Kyu Kim, Kee Nam Song, and Yeon Ho Jung
Korea Atomic Energy Research Institute
150 Dukjin-dong Yusong-gu, Taejon 305-353, Korea
khyoon@kaeri.re.kr

(Received June 19, 2000)

Abstract

The spacer grid is one of the main structural components in the fuel assembly, which supports the fuel rods, guides cooling water, and protects the system from an external impact load, such as earthquakes. Therefore, the mechanical and structural properties of the spacer grids must be extensively examined while designing them. In this paper, a numerical method for predicting the buckling strength of spacer grids is presented. Numerical analyses on the buckling behavior of the spacer grids are performed for a various array of sizes of the grids considering that the spacer grid is an assembled structure with thin-walled plates and imposing proper boundary conditions by nonlinear dynamic finite element method using ABAQUS/Explicit. Buckling tests on several numbers of specimens of the spacer grid were also carried out in order to compare the results between the test and the simulation result. The drop test is accomplished by dropping a carriage on the specimen at a pre-determined position. From this test, the specimens are buckled only at the uppermost and the lowermost layer among the multi-cells, which is similar to the local buckling at the weakest point of the grid structure. The simulated results also similarly predicted the local buckling phenomena and were found to give good correspondence with the experimental values for the thin-walled grid structures.

Key Words : critical impact force, buckling, thin-walled structure, impact velocity, drop test, strain localization

1. Introduction

The spacer grid, one of the most important components of a nuclear fuel assembly, is composed of straps, which are crossed to form an egg-crate like structure. It constitutes the skeleton of the fuel assembly together with guide thimbles, top and bottom end pieces. The structural grid assemblies provide both lateral and vertical support for the fuel rods. The pitch of the fuel

rods in the core is a carefully selected parameter, which has a major effect on the nuclear and thermal/hydraulic performance of the core. The spacer grid is an interconnected array of slotted grid straps welded at the intersections. The fuel assembly incorporates from seven to eleven spacer grids. The spacer grid outer straps constitute the contact surfaces that can transmit possible seismic loads between the fuel assemblies. The principal design concern with regard to grid strap buckling is that the fuel rods should maintain a coolable geometry and that the control rods should be inserted [1].

The design practice is to adopt the incipient buckling load as a failure criterion for the grid. The diagonal axis of the grid assembly has the lowest impact strength. Sustained loads applied along the diagonal axis, however, are not credible because slipping between grid assemblies causes diagonal loads to be applied to the grids in normal directions only.

Consequently, the limiting loads imposed upon the grid assembly are the result of impacts due to lateral seismic accelerations, lateral LOCA (Loss Of Coolant Accident) blowdown forces, and shipping and handling loads. The ability of the grid to resist lateral loads is characterized in terms of its dynamic and static crush strengths. These quantities and the grid dynamic stiffness are required for fuel assembly seismic and LOCA blowdown analyses to verify that the coolable grid geometry is maintained.

During the calculations, the cutout section is not regarded to affect the buckling strength. The dynamic impact properties (dynamic stiffness and coefficient of restitution) are determined by measuring the impact force and its duration as a function of impact velocity, with suitable assumptions.

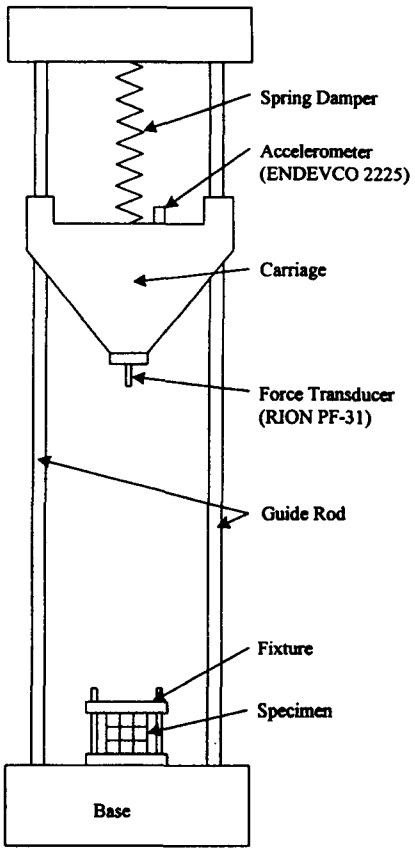

Fig. 1. Schematic Diagram of the Free Fall Type Shock Machine

2. Drop test

2.1. Test Apparatus Setup

A free fall type shock machine, as shown in Figure 1, is used to perform the tests. It is intended to simulate the type of load and impact velocities anticipated under a seismic disturbance. The upper part of the structure consists of two guide rods and supporting columns, which are erected from the base. The carriage moves with the guidance of the two guide rods. The carriage is made of aluminum casting, the shape of which is

determined for obtaining the maximum rigidity with minimum mass.

The general test setup consists of the floor, dummy weight, force transducer, dynamic accelerometer, and mounting fixtures [2]. The impact force by the carriage is found too high to investigate the critical buckling load of the grid structure. Therefore, an additional spring damper is mounted on the top surface of the carriage in order to decrease the impact velocity. The total moving mass is 23.5 kg, which contains the carriage, sensor, and spring damper. The force transducer is mounted on the bottom surface of the carriage to measure the impacting forces. One dynamic accelerometer is mounted on the top surface of the carriage.

The grids are rigidly clamped to the holding plate that is also placed on the floor. The initial drop height of the impact weight is 1.75 inches (44.45 mm). The impacting tests were performed on 3×3 array grids. The grids are fixed to the holding fixture by 4 screws. The carriage is moved to the initial height and then dropped onto the grid. This procedure is repeated, increasing the height by 0.25 inches (6.35 mm) at each step until the specimen buckles.

2.2. Test Specimen and Impact Velocity Calculation

In the impact test machine, there is no amplifier with a direct time integration algorithm for calculating the impact velocity during the impact test. Therefore, a simple equation is derived from the energy equilibrium of the test apparatus. This energy equilibrium state is shown in Figure 2.

The acceleration signal is shown as a half-sine wave during the impact time. The equation for the calculation of the critical impact velocity is induced using the energy and force equilibrium conditions. The impact velocity is evaluated using this equation. The induced equation is as follows.

From the energy conservation principle,

$$-mg(x_0 - l) + \tfrac{1}{2}k(x_0 - l)^2 = \tfrac{1}{2}mv^2 - mg(x_0 + h) + \tfrac{1}{2}k(x_0 + h)^2 \quad (1)$$

From the force equilibrium condition of the system,

$$mg = kx_0 \quad (2)$$

Substitute Eq. (2) into Eq. (1) and the impact velocity is as follows.

$$v = \sqrt{\frac{k}{m}(l^2 - h^2)} \quad or \quad \omega_n\sqrt{(l^2 - h^2)} \quad (3)$$

Where the natural frequency of the system is about 1.27, the averaged critical acceleration and impact force by the impact test are at a 3.5 inch (0.089 m) drop height; the signal by the test definitely shows that grid buckling occurs. Hence, the critical impact velocity using Eq. (3) is about 0.38 m/sec.

The specimens for the impact test are made of

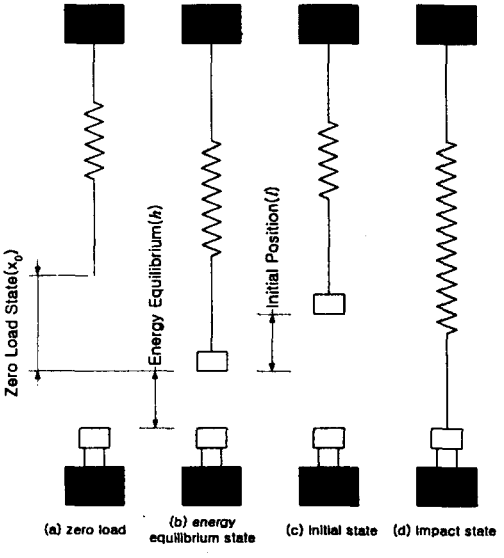

Fig. 2. Schematic View for the Impact Velocity Calculation

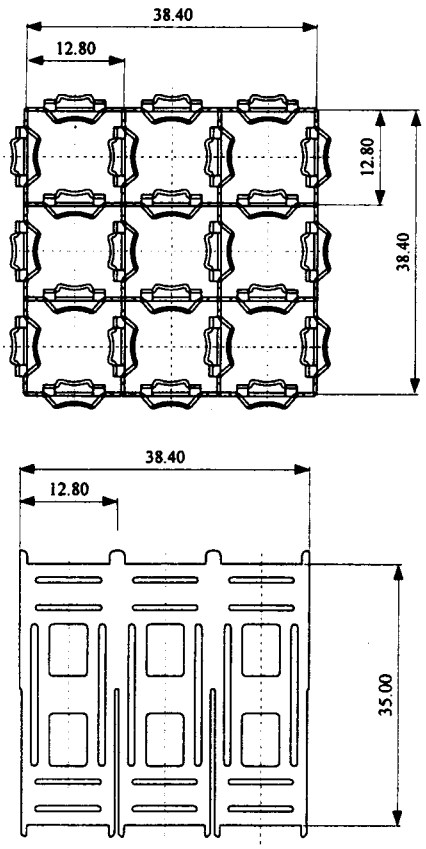

Fig. 3. Schematic Drawing of the 3×3 Cell Grid Structure

stainless steel and the plate thickness is 0.6 mm. Most of the materials for the spacer grid are used with Zircaloy or Inconel. However, since this is only a candidate model, the stainless steel material is used. These rectangular plates have some cutouts with a complicated shape. The unit plates are inserted in each other and welded at the cross-point and contact surface to compose the grid cell using the laser welding procedure. A schematic drawing of the H type 3×3 cell grid structure is shown in Figure 3.

2.3. Test Results

The impact force and acceleration during the test is a half sine signal in the time domain. This time-history data is obtained from the drop test and shown in Figure 4.

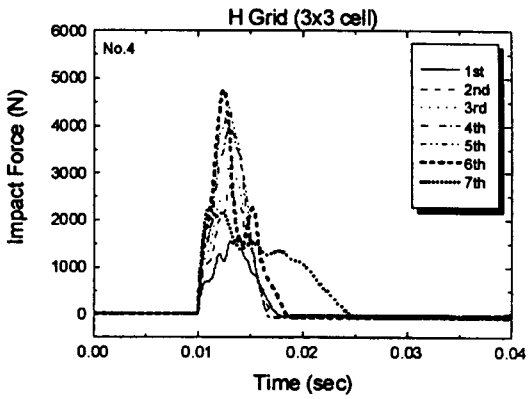

Fig. 4. Time-history Data of the 3×3 Cell Grid by the Impact Test

If some grid cells experience local buckling, the duration time is longer than before the buckling state. This means that the stiffness of the grid structure after buckling is much smaller than before the buckling phenomena. As a test result, the normal duration time is 6 to 8 milliseconds as the geometry of the specimen. The impact force range of the H type 3×3 cell grid specimen at the buckling point is from 3474 N to 6402 N and the impact acceleration range is from 14.1 g to 25.8 g. These variations were caused by the difference of the geometrical dimension and residual stress by welding as the specimen and non-uniform contact surface between impact hammer and top surface of the specimen. The average values are 5122 N and 20.6 g, respectively. The results of the test are summarized in Figure 5.

A representative deformed shape of the specimen is shown in Figure 6. In this Figure, only the uppermost and lowermost cells of the grid are buckled, but the middle layer cells of the grid retain their original shape. That the local buckling is concentrated at the cross point of the grid structure and these cross points is why the

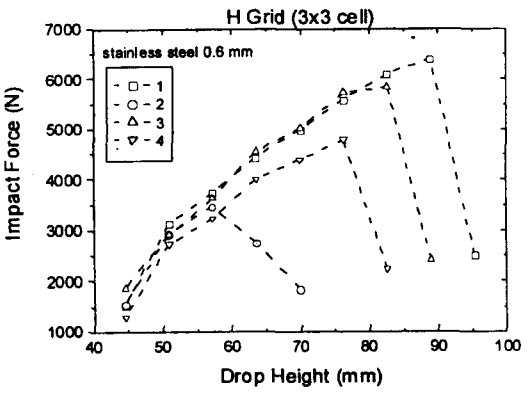

Fig. 5. Test Results of the 3 × 3 Cell Grid Structures

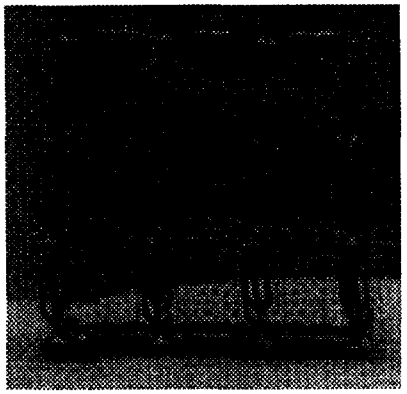

Fig. 6. Buckling Mode Shape of the 3 × 3 Cell Grid Structures by Dynamic Impact Tests

maximum strain of the global structure appeared at these areas [3]. Even though the equivalent plastic strain is different for the number of cells, the maximum equivalent stress is nearly the same.

3. Nonlinear Dynamic Impact Analysis

3.1. FE Model and Boundary Conditions

The nonlinear dynamic impact analysis is simulated by a finite element method. The commercial code ABAQUS/Explicit (version 5.8) is used for the FE analysis [4]. The geometrical data for the FE analysis follow the specimen of the 3 × 3 cell grid with steel as shown in Figure 3. In the analysis, the calculation involves 20 steps and the time step width is 2 milliseconds, so the total analysis time is 40 milliseconds. Besides the geometry, 186.8 GPa is used for Young's modulus of the grid material, stainless steel. 0.3 is used for the Poisson ratio. Since the characteristic curve shows nonlinear elastic-plastic behavior, the plastic property of the material is also considered, such as the yield strength (258.6 MPa) and the hardening curve. The stress vs. strain curve of stainless steel for the dynamic analysis is applied.

4-node shell elements are used for the FE model of the analyses. The impact hammer is modeled as the rigid surface with a mass element which is the same hammer weight. For the boundary conditions of the FE analysis, three translational degrees of freedom at the lower four edges are constrained since the specimen is regarded to have simply supported conditions on the edges of the grid specimen during the dynamic impact test. The number of elements is 2352, and the number of nodes is 3296. This FE model is well described in Figure 7.

The imposed initial velocity onto the rigid surface, which initially contacts the top of the grid, simulates the dynamic impact load onto the grid. This rigid surface is offset as half of the shell thickness, 0.3 mm. This rigid surface only contacts the top surface of the structure. After impact with the structure, the rigid surface rebounds in the reverse direction of the structure. The applied boundary conditions are shown in Figure 8 [4, 5].

The imposed external force is the initial velocity on the center node of the rigid surface using the initial velocity condition. The impact force of the grid is obtained from the total reaction force at

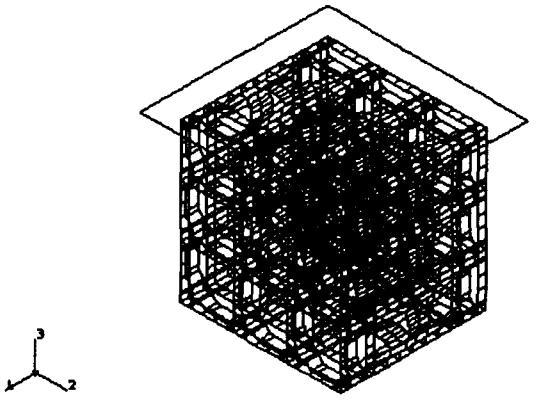

Fig. 7. FE Model for Nonlinear Impact Analysis

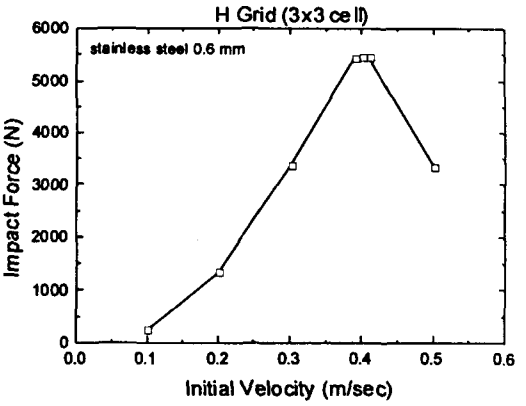

Fig. 9. Impact Force of the 3×3 Cell Grid Structure with the Initial Impact Velocity

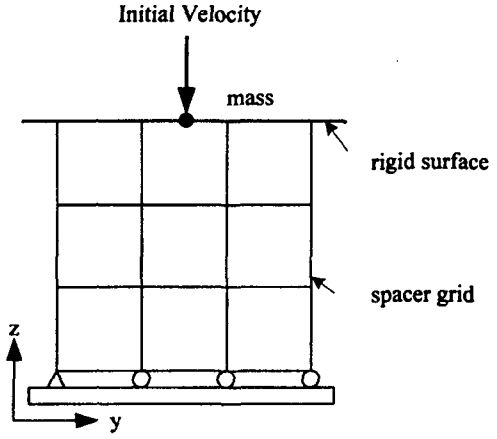

Fig. 8. Boundary Conditions for Dynamic Impact Analysis

the displacement constrained four lower edges by applying the initial velocity on the rigid surface. If the reaction force at the present step is smaller than the previous analysis step, the critical impact value is between the present and previous step. In order to find the critical impact velocity, the increment initial velocity is reduced in the vicinity of 10 % of the current value. Finally, the critical impact velocity is determined as the above analysis step.

3.2. Analysis Results

The FE results for simulating the dynamic impact characterization curves are given in Figure 9. In this Figure, the critical impact velocity is 0.40 m/sec. This value is in good correspondence with the test results. The impact force increases until the buckling of a grid cell occurs.

When the initial velocity leads to the critical impact velocity, local buckling occurs only at the uppermost and lowermost cells of the grid. The difference in the impact force between the test and the analysis is - 6.5 %. The difference in the critical impact velocity between the test and the analysis is - 5.3 %. The maximum stress is revealed at the corner leg of the unit cell as shown in Figure 10.

These areas only appear at the uppermost and lowermost cells. Therefore, the grid structure collapses if any cells of the grid begin to yield locally. It appears logical to design a lacing system so that its members are just strong enough to carry the shearing forces, which arise when a deflection reaches the magnitude at which the chord on the concave side of the bent plate begins

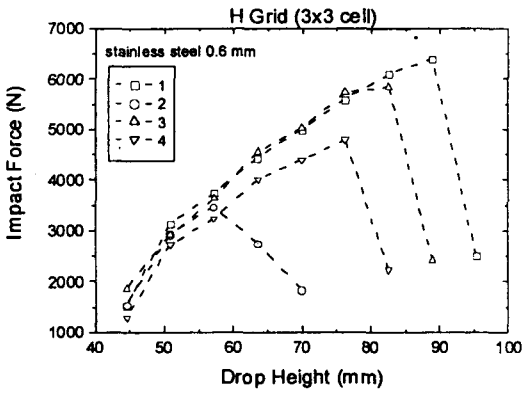

Fig. 5. Test Results of the 3 × 3 Cell Grid Structures

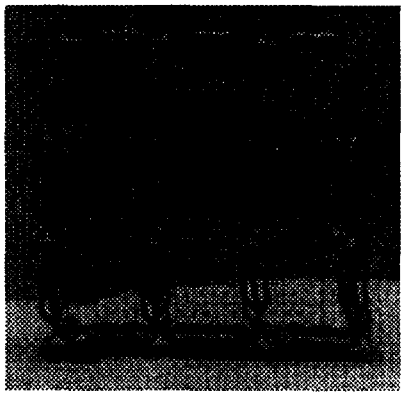

Fig. 6. Buckling Mode Shape of the 3 × 3 Cell Grid Structures by Dynamic Impact Tests

maximum strain of the global structure appeared at these areas [3]. Even though the equivalent plastic strain is different for the number of cells, the maximum equivalent stress is nearly the same.

3. Nonlinear Dynamic Impact Analysis

3.1. FE Model and Boundary Conditions

The nonlinear dynamic impact analysis is simulated by a finite element method. The commercial code ABAQUS/Explicit (version 5.8) is used for the FE analysis [4]. The geometrical data for the FE analysis follow the specimen of the 3 × 3 cell grid with steel as shown in Figure 3. In the analysis, the calculation involves 20 steps and the time step width is 2 milliseconds, so the total analysis time is 40 milliseconds. Besides the geometry, 186.8 GPa is used for Young's modulus of the grid material, stainless steel. 0.3 is used for the Poisson ratio. Since the characteristic curve shows nonlinear elastic-plastic behavior, the plastic property of the material is also considered, such as the yield strength (258.6 MPa) and the hardening curve. The stress vs. strain curve of stainless steel for the dynamic analysis is applied.

4-node shell elements are used for the FE model of the analyses. The impact hammer is modeled as the rigid surface with a mass element which is the same hammer weight. For the boundary conditions of the FE analysis, three translational degrees of freedom at the lower four edges are constrained since the specimen is regarded to have simply supported conditions on the edges of the grid specimen during the dynamic impact test. The number of elements is 2352, and the number of nodes is 3296. This FE model is well described in Figure 7.

The imposed initial velocity onto the rigid surface, which initially contacts the top of the grid, simulates the dynamic impact load onto the grid. This rigid surface is offset as half of the shell thickness, 0.3 mm. This rigid surface only contacts the top surface of the structure. After impact with the structure, the rigid surface rebounds in the reverse direction of the structure. The applied boundary conditions are shown in Figure 8 [4, 5].

The imposed external force is the initial velocity on the center node of the rigid surface using the initial velocity condition. The impact force of the grid is obtained from the total reaction force at

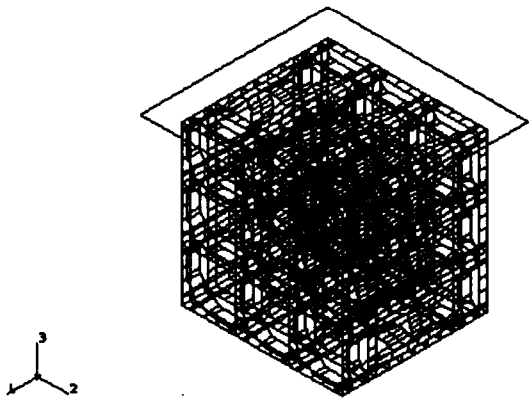

Fig. 7. FE Model for Nonlinear Impact Analysis

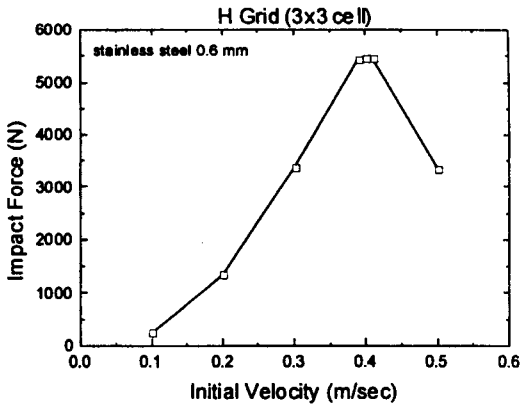

Fig. 9. Impact Force of the 3×3 Cell Grid Structure with the Initial Impact Velocity

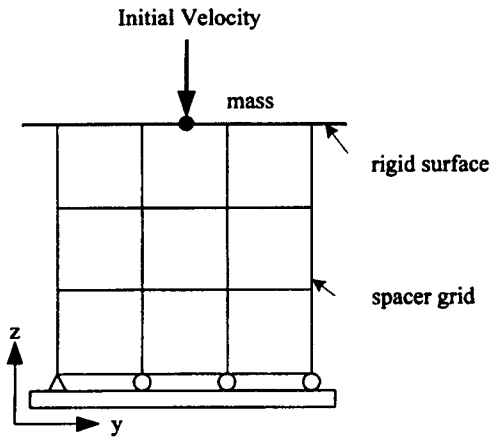

Fig. 8. Boundary Conditions for Dynamic Impact Analysis

the displacement constrained four lower edges by applying the initial velocity on the rigid surface. If the reaction force at the present step is smaller than the previous analysis step, the critical impact value is between the present and previous step. In order to find the critical impact velocity, the increment initial velocity is reduced in the vicinity of 10 % of the current value. Finally, the critical impact velocity is determined as the above analysis step.

3.2. Analysis Results

The FE results for simulating the dynamic impact characterization curves are given in Figure 9. In this Figure, the critical impact velocity is 0.40 m/sec. This value is in good correspondence with the test results. The impact force increases until the buckling of a grid cell occurs.

When the initial velocity leads to the critical impact velocity, local buckling occurs only at the uppermost and lowermost cells of the grid. The difference in the impact force between the test and the analysis is - 6.5 %. The difference in the critical impact velocity between the test and the analysis is - 5.3 %. The maximum stress is revealed at the corner leg of the unit cell as shown in Figure 10.

These areas only appear at the uppermost and lowermost cells. Therefore, the grid structure collapses if any cells of the grid begin to yield locally. It appears logical to design a lacing system so that its members are just strong enough to carry the shearing forces, which arise when a deflection reaches the magnitude at which the chord on the concave side of the bent plate begins

Table 1. Comparison Between the Test and Analysis Results

Classification	Critical impact strength	Critical impact velocity
Drop test (Average value)	5122 N	0.38 m/sec
Non-linear dynamic analysis	5457 N	0.40 m/sec
Deviation	- 6.54 %	- 5.26 %

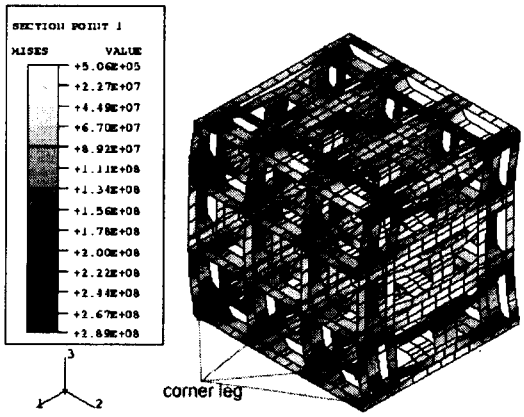

Fig. 10. Von Mises Equivalent Stress Contour by Nonlinear Impact Analysis

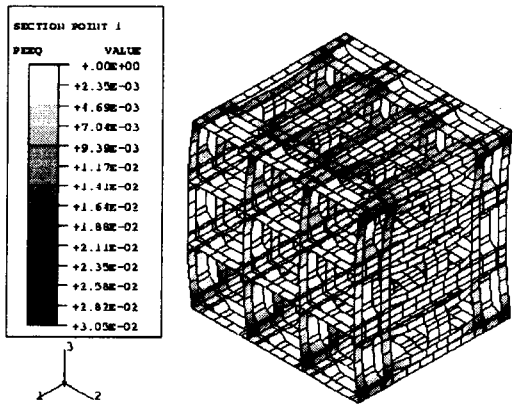

Fig. 11. Equivalent Plastic Strain Contour by Nonlinear Impact Analysis

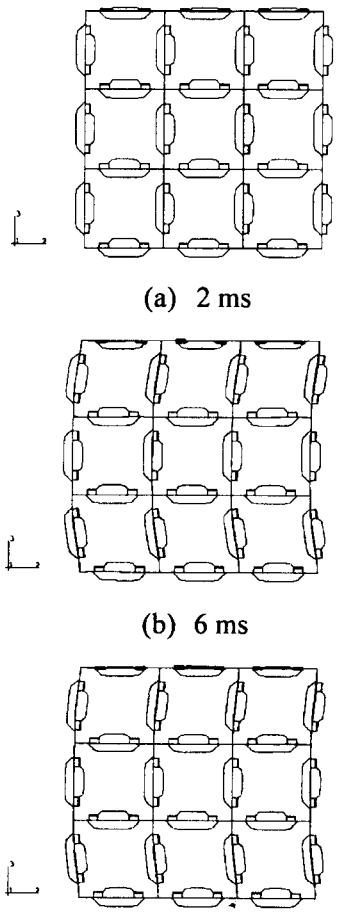

Fig. 12. Deformed Shape of a 3 × 3 Cell Grid by Nonlinear Dynamic Impact Analysis

to yield. The highest stressed parts of the grid will then yield or collapse simultaneously [6]. The equivalent plastic strain is shown in Figure 11. In Figure 12, the strain localization phenomenon

remarkably appears at the corner leg of the grid [7].

The deformed shape is very similar to the test results, which are shown in Figure 6. The deformed shape in the elastic region tends to return to the original shape by strain localization. The elastic unloading phenomenon is shown well in this Figure. In Table 1, the analysis results are compared with the test results.

4. Discussion and Conclusions

4.1. Buckling Behavior of the Grid Tructure

The buckling parameter, as the critical buckling strength, and the deformed shape as a function of time, are similar to those of the shock test. The reason for local buckling is considered to be the strain localization of the plastic hinge, which is located in the vicinity of the welding nugget. If there is plastic deformation, the stiffness of the material at the plastic region should be locally much lower. The nonlinear dynamic impact analysis for the spacer grid is conducted and the intrinsic boundary condition of the grid structure is checked. The importance of the boundary conditions is apparently verified by using several boundary conditions. It seems that the difference is caused by the geometry of each specimen. Comparing the analysis results with the test results defines the boundary conditions finally applied. The analysis results correspond well with the test results and can predict the critical buckling strength and impact velocity. Therefore, this FE model and analysis procedure will be used as a tool for predicting the nonlinear buckling behavior of the grid structures.

The drop test shows some of the grid' s the interesting buckling. The deviation bounds of the impact force and acceleration by the test are within ± 30 %. The buckling of the grid initiates at

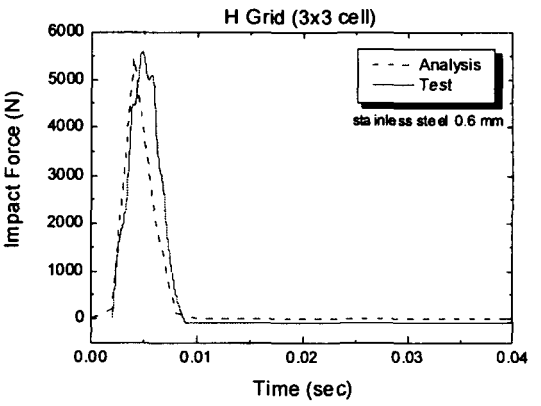

Fig. 13. Comparison Curve of Critical Impact Corce Between Test and Analysis Result

only the uppermost and lowermost cells, but the middle layer of cells retains its original shape. It is the weakest layer cell of a grid, which initiates buckling in the shear direction by the strain localization phenomenon.

In Figure 13, the critical impact force of a 3×3 cell grid structure is plotted. The buckling behavior of a 3×3 cell grid structure by nonlinear dynamic impact analysis is in good agreement with the test result.

4.2. Conclusion and Future Research

The present paper deals with the lateral buckling of a grid structure, which is composed of thin-walled plates. A drop test was executed by dropping a carriage onto the specimen. A factor governing the buckling of the grid structure is the local buckling of a unit cell.

This local buckling occurred at the maximum strain over the yield strain of the material. The following points are left as future problems: The buckling behavior of the grid structure under the operating temperature and the strain localization phenomena in connection with the size of the elements in the grid structure.

Acknowledgement

This work was financially supported by the nuclear R&D program from the Ministry of Science and Technology of Korea.

References

1. K. H. Yoon, K. N. Song and K. H. Choi, FE Analysis of Nonlinear Buckling Behavior of a Grid Structures, *Proceedings of the KSME 1999 Fall Annual Meeting A*, Korea, Paper No. 99F077, (1999).
2. C. M. Harris, Shock and Vibration Handbook, 4th ed., McGraw-Hill Book Co., (1996).
3. K. H. Yoon, K. N. Song and H. B. Kim, Nonlinear Dynamic Lateral Buckling Behavior of a Grid Structures, *Proceedings of the KSME 2000 Spring Annual Meeting A*, Korea, Paper No. 00S044, (2000).
4. H. D. Hibbitt, G. I., Karlsson, and E. P. Sorensen, ABAQUS/Explicit User's Manual (version 5.8), Vol. I and II, Hibbitt, Karlsson & Sorensen Inc., Pawtucket, R.I., USA, (1998).
5. K. H. Choi, et al., FE Analysis of Nonlinear Buckling Behavior of a Spacer Grid in Fuel Assembly, *Structural Mechanics in Reactor Technology, SmiRT-15*, Seoul, Korea, Paper No. C02/3, (1999).
6. B. Friedrich, Buckling Strength of Metal Structures, McGraw-Hill Book Company, NY, (1952).
7. P. B. Zdenek, L. Cedolin, Stability of Structures : Elastic, Inelastic, Fracture, and Damage Theories, Oxford University Press, (1991).